Electrochemical Synthesis of a Multipurpose Pt–Ni Catalyst for Renewable Energy-Related Electrocatalytic Reactions

Md Abu Sayeed,[a, b] Charlotte Woods,[a] Jonathan Love,[a, b] and Anthony P. O'Mullane*[a, b]

Renewable energy driven electrochemical processes are becoming increasingly important in the transition away from fossil fuels. One of the key reactions is electrochemical water splitting to generate green hydrogen which ideally could be directly integrated with a wind or solar electricity source. However, alkaline electrolysers suffer from significant degradation in performance if they are rapidly powered down under reduced sunlight conditions when directly coupled with a solar cell due to reverse current flow. In this work we address this issue by creating a truly bifunctional electrode material that is switchable between the hydrogen evolution reaction (HER) and the oxygen evolution reaction (OER). The synthesis method is simple whereby a Pt electrode is electrochemically activated and then immersed in a nickel nitrate solution to electrolessly deposit Ni on the surface. When this electrode is electrochemically cycled, it creates an active Pt–Ni alloy at the Pt surface. Importantly, this electrocatalyst is switchable between both reactions without loss of activity as evidenced by an accelerated stress test over a 24 h period. An added advantage is that this Pt–Ni electrocatalyst is also more active than Pt for the oxygen reduction reaction which opens up its applicability in fuel cells. Finally, to demonstrate the multifunctionality of this Pt–Ni material, ethanol and ammonia oxidation is demonstrated which also shows better performance than Pt.

1. Introduction

Electrochemical water splitting to produce green hydrogen is considered one of the most promising technologies to meet the world's future energy demand while minimizing the energy sector's carbon footprint. The attractiveness of generating hydrogen at scale is that it may eventually allow for seasonal storage of renewable energy that is then available on demand to realize a hydrogen society.[1] However, there are still issues associated with the cost of electrode materials, long term stability and the ability to directly integrate electrolysers with intermittent renewable energy sources and smart grid systems.[1c] Therefore, a significant effort is underway to improve electrolyser performance.[1b,2]

Platinum is an excellent catalyst which is highly effective for a variety of important electrocatalytic reactions such as the hydrogen evolution reaction (HER) involved in electrochemical water splitting. In addition, Pt is a proven material for fuel cell relevant reactions such as the oxygen reduction reaction (ORR), ethanol oxidation reaction (EOR) and the ammonia oxidation reaction,[3] which are critical for the generation of clean electricity as well as ensuring the possibility of a zero carbon footprint for the transportation industry. The ammonia oxidation reaction is also gaining significant attention as an alternative fuel for use in fuel cells[3g,4] given the recent emergence in clean electrochemical ammonia synthesis.[5]

A problematic issue for Pt is cost and therefore large scale roll out of commercial electrochemical devices based on Pt is prohibitive. Therefore, research on specific strategies to increase Pt atom utilization efficiency is ongoing which has been successfully demonstrated for fuel cell relevant reactions where Pt is alloyed with another metal or multiple metals.[6] An added advantage of Pt alloys and bimetallic materials is that it improves the catalyst's tolerance to poisoning during organic molecule oxidation reactions.[7] One particularly effective electrocatalyst is Pt_3Ni which shows enhanced performance for the ORR compared to Pt due to weakening of intermediate species created during the reaction due to an unusual electronic structure and d-band centre position.[8] However its applicability for other electrocatalytic reactions are not widely reported. This is somewhat surprising as the combination of Ni and Pt is expected to be beneficial for many electrocatalytic reactions. Recently it has been reported that Ni deposited on Pt(111) surfaces lowers the barrier for hydrogen adsorption in alkaline solutions and enhances the HER,[9] while Ni single atoms on Pt can also improve the HER and encouragingly showed activity towards methanol oxidation.[3b] Markovic reported that for ultrathin $Ni(OH)_2$ on Pt, that the edges of $Ni(OH)_2$ promoted the dissociation of water and release of hydrogen intermediates which subsequently adsorbed on the nearest Pt surface and recombined into molecular hydrogen.[10] The use of Ni should in principle open up applicability for the OER as Ni and its various oxides/hydroxides have been shown to be excellent catalysts for this reaction.[11] Markovic also reported that 3*d*-M hydr(oxy) oxides (Ni, Co, Fe, Mn) supported on Pt(111) surfaces were active for the HER and OER.[12] Therefore creating a multifunctional electrocatalyst based on the Pt/Ni system should be achievable.

[a] Dr. M. Abu Sayeed, C. Woods, Dr. J. Love, Prof. A. P. O'Mullane
School of Chemistry and Physics
Queensland University of Technology (QUT)
Brisbane, QLD 4001, Australia
E-mail: anthony.omullane@qut.edu.au
[b] Dr. M. Abu Sayeed, Dr. J. Love, Prof. A. P. O'Mullane
Centre for Clean Energy Technologies and Practices
Queensland University of Technology (QUT)
Brisbane, QLD 4001, Australia

Supporting information for this article is available on the WWW under https://doi.org/10.1002/celc.202001278

One method that has been explored previously is the use of electrochemically activated electrodes that allow for subsequent electroless deposition of less noble metals on the surface. The creation of active surfaces that are readily oxidized allows for the spontaneous deposition of metals from their salts that are not thermodynamically favoured when the standard reduction potentials of the relevant metal/metal ion couples are considered. This has been shown for the deposition of Ag onto electrochemically activated Au to generate an Ag/Au electrode.[13] This has also been classified as an "anti-galvanic replacement" reaction where the formation of Cu on Ag nanoclusters has been observed.[14] This approach allows for the creation of an active surface with excellent homogeneous decoration of a second metal and avoids large isolated nanoparticle formation thereby enhancing atom efficiency,[13] which is often encountered with conventional electrodeposition.

In this work the aim was to generate a bifunctional Pt–Ni surface via this approach and investigate its behaviour towards overall water splitting. A newly developed accelerated ageing test mimicking the rapid shut down and start up conditions of an electrolyser indicated that the catalyst maintained its activity. Promisingly, the Pt–Ni electrode showed excellent activity for the ORR while also demonstrating electrocatalytic effects for ethanol and ammonia oxidation reactions.

2. Results and Discussion

2.1. Electrochemical Water Splitting

The method chosen to activate the Pt electrode was polarization in the hydrogen evolution region in 1 M H_2SO_4. Previous studies have demonstrated that this is a highly effective way to generate active adatom sites on electrode surfaces that oxidize at potentials well below the thermodynamic potential for Pt oxide formation.[14] This method produces metastable surface states with atoms of low coordination number that are highly reactive and therefore can be readily oxidised. Koper has shown that under severe polarization conditions that the creation of nanoparticles from a bulk wire is even possible.[16] In addition the formation of platinum hydride is likely to occur which offers another potential route for Ni decoration via partial replacement at the adatom scale. A typical polarisation curve is shown in Figure S1 demonstrating a noisy response due to vigorous gas evolution. After this electrochemical activation process the electrode was transferred into degassed water to minimise oxidation of the surface followed by rapidly immersing the electrode into a $Ni(NO_3)_2.6H_2O$ solution at different concentrations for different times. The modification process was optimised to achieve the best OER and HER performance (Figure S2) which resulted in a 1 minute cathodic polarisation activation time followed by immersion in 5 mM $Ni(NO_3)_2.6H_2O$ for 3 minutes. A variety of samples were then produced including a Pt rotating disk electrode (RDE) and electrodeposited Pt on a GC electrode as outlined in Table 1 (see Experimental Section).

Table 1. Fabrication conditions for the electrocatalyst samples.

Sample	Substrate	Pt type / treatment	Ni addition procedure
S-0	Pt RDE	None	None
S-1	Pt RDE	Cathodic polarisation	None
S-2	GC RDE	Electrodeposited Pt on GC electrode followed by cathodic polarisation	Electroless deposition
S-3	Pt RDE	None	Electroless deposition
S-4	Pt RDE	Cathodic polarisation	Electroless deposition

To study changes in the electrochemical behaviour of the Pt electrode, cyclic voltammetry was undertaken in 1 M KOH. Figure 1a shows typical cyclic voltammetric behaviour for polycrystalline Pt (sample S-0),[16] i.e., the H_{ads}/H_{des} region from −0.25 V to 0.40 V followed by a broad Pt oxide formation process from 0.50 to 1.30 V and its subsequent reduction with a peak at 0.71 V on the cathodic sweep. For sample S-4 there is a slight change in the H_{des} profile in the anodic scan with a more pronounced peak at 0.035 V which is related to the oxidation of more molecular hydrogen generated in the cathodic sweep[16] compared to sample S-0. This is followed by an anodic peak at 1.2 V which is often indicative of oxygen adsorption at Pt(111) sites.[16] There is also a slight positive shift of 10 mV in the Pt oxide reduction peak which indicates slightly weaker oxygen adsorption at the Pt–Ni electrode compared to Pt which can have implications for the ORR.[8c] Upon increasing the potential window (Figure 1b) to 1.6 V a new process appears on the Pt–Ni electrode which is related to the redox processes associated with Ni at 1.41 V prior to the onset of the OER towards the end of the sweep. On the cathodic sweep there is an increase in the magnitude of the current response from 1.0 V to the end of sweep which is due to the overlapping reduction of oxygen liberated in the anodic sweep. From this data it indicates that modification of the Pt electrode with Ni does not result in any significant change in the surface area of the electrode.

Figure 2 shows the HER and OER performance in 1 M KOH for the different electrodes (Table 1). It shows that Pt is inactive for the OER (Sample S-0) as expected and it is only after both

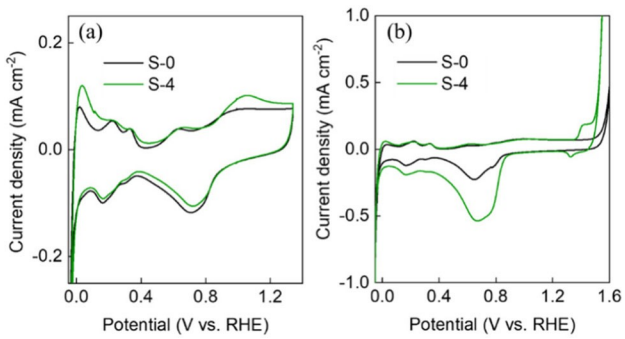

Figure 1. Cyclic voltammograms recorded at 50 mV s^{-1} in 1 M KOH for sample S-0 and S-4 over the potential range of a) −0.25 to 1.25 V and b) −0.25 to 1.6 V.

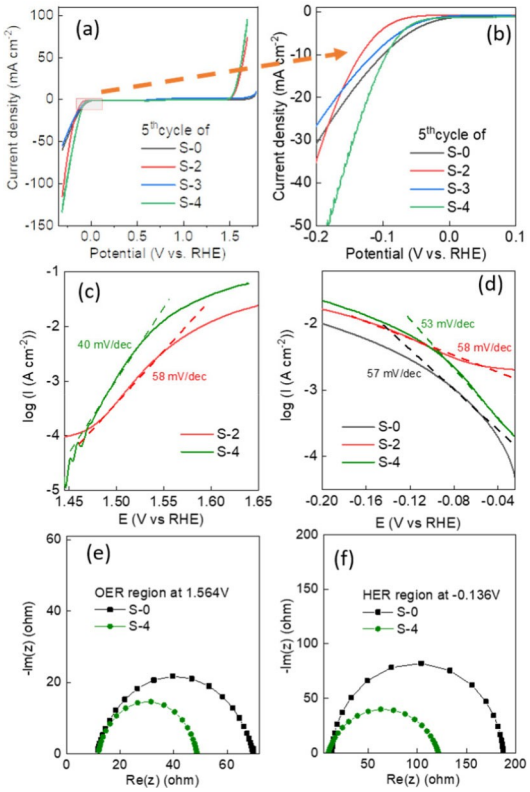

Figure 2. Cyclic voltammograms obtained at 20 mV s^{-1} showing a) OER and HER performance for different samples, b) enlarged HER performance of the samples; Tafel slope obtained at 1 mV s^{-1} in c) OER region and d) HER region; Nyquist plots of e) OER and f) HER.

cathodic polarization activation and immersion in $Ni(NO_3)_2.6H_2O$ that OER activity is observed (Sample S-4), attributed to the formation of Ni on the surface (as confirmed by XPS, TEM and discussed below). To determine if Pt activation is required for the formation of Ni and hence OER activity, a polished Pt RDE was immersed in $Ni(NO_3)_2.6H_2O$ (Sample S-3), however no activity was observed. This phenomenon was also studied for Pt electrodeposited onto a GC electrode (Sample S-2) where the OER was comparable to that seen for the Pt RDE case (Sample S-4). The Tafel slope for the OER for samples S-2 and S-4 (Figure 2c) are 58 and 40 mV dec^{-1} respectively indicating the slightly better performance of the Ni decorated Pt RDE system. This is also reflected in the overpotential required to pass 10 mA cm^{-2} which was 300 and 330 mV for samples S-4 and S-2 respectively. EIS was also undertaken at a potential in the OER region for samples S-0 and S-4 (equivalent circuit is shown in Figure S3) where the R_{ct} value were 59 and 38 Ω respectively (Figure 2e), indicating improved electron transfer kinetics for Pt–Ni compared to Pt.

For the HER, there is a significant increase in the current density passed for samples S-2 and S-4, indicating that the presence of Ni on Pt is highly beneficial. Although the onset potential for these samples is slightly more negative (ca. 20 mV more negative for sample S-4) than unmodified Pt (Sample S-0) (Figure 2b) the ability to pass significantly higher current at overpotentials greater than 0.08 V is of importance from a commercial point of view which requires much higher current densities than the often quoted 10 mA cm^{-2} in the literature. The slightly more negative onset potential may be due the extent of coverage of $Ni(OH)_2$ on the surface which affects the bifunctional mechanism that requires water dissociation at the $Ni(OH)_2$ site followed by hydrogen adsorption and association on the free Pt sites to liberate hydrogen.[18] For the HER, the Tafel slopes for the Ni modified electrodes are quite similar to Pt where values of 53, 58 and 57 mV dec^{-1} were recorded for samples S-4, S-0 and S-2, respectively (Figure 2d). This shows that the mechanism for the HER is not changed upon inclusion of Ni into the system but its presence does facilitate greater hydrogen evolution at potentials beyond −0.08 V. EIS was also undertaken for samples S-0 and S-4 where the presence of Ni shows a decrease in impedance in the system and the charge transfer resistance (R_{ct}) value decreases from 173 Ω to 111 Ω (Figure 2f) indicating a more facile reaction at sample S-4. Sample S-1, which is an activated Pt RDE but not decorated with Ni, did not show any OER activity or improvement in the HER over a polished Pt RDE and therefore the data is not shown.

The stability of sample S-4 was then studied to see if it could be switched between the HER and OER without loss of activity (Figure 3a) which shows only a very slight decrease in OER and HER currents after 1000 cycles. The sweep rate for this experiment was increased to 100 mV s^{-1} to allow the redox features before the onset of the OER to be observed. The anodic peak is attributed to the oxidation of Ni^{2+} species to Ni^{3+} at ca. 1.32 V while the reverse reaction occurs at ca. 1.28 V where the potentials for these processes are consistent with NiO and $Ni(OH)_2$ electrocatalysts.[11c,17] Interestingly, there is a continuous shift in potential for this redox process prior to the OER to more positive values upon repetitive potential cycling (Figure 3b). This shift is not observed for Ni oxide/hydroxide materials and usually a slight drop in intensity of the signal occurs upon cycling.[11c,18] A shift of this type is typically indicative of a doping or alloying effect occurring at the electrode,[21] and suggests there may be an interaction between the surface Ni and underlying Pt. The possibility that this is an Fe contaminant which can also influence the oxidation potential of Ni oxides was ruled out. The presence of Fe is

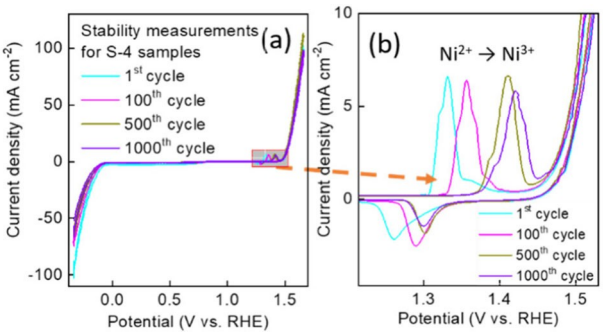

Figure 3. a) Cyclic voltammograms recorded in 1 M KOH for 1000 cycles at 100 mV s^{-1} for sample S-4, b) enlarged region showing the Ni oxidation process.

usually reflected in a reduction in magnitude of the redox process with a concomitant increase in OER current.[22] Here we do not see any reduction in the intensity of the Ni oxide oxidation process and the OER current only changes marginally during 1000 cycles. In addition, Fe was not detected in the sample by XPS or EDS analysis in the TEM. Therefore, it appears that there is a significant interaction between the surface Ni and the underlying Pt due to repetitive potential cycling.

Commercial electrolysers generally need to be operated at a base load to minimize the phenomenon of reverse current flow that occurs upon shutdown or ramp up.[23] The Pt–Ni catalyst was therefore tested to ascertain if it would be tolerant to rapid shutdown and start up conditions by applying a potential waveform that switched between the OER, HER and to potentials where no Faradaic reaction occurred. The timescale for each step was varied from 5 min over a 1 h period to 1 h steps over a 24 h period and is shown in Figure 4a and b respectively. Interestingly, the OER stabilizes quickly within 1–2 min to reach a steady value, whereas the HER takes longer at ca. 10 min. The large changes in current at the beginning of each step are related to double layer charging. Promisingly, even after rapid switching between the HER, OER and potentials where no electrochemical reaction is taking place (mimicking shut down conditions) the OER and HER current densities remain consistent across the 24 h time period. This type of accelerated ageing testing certainly illustrates the excellent bifunctional behaviour of this electrode material to water electrolysis. The stability of our system is highly promising as it is better than that reported previously using commercial electrodes, such as Pt for the cathode and IrO_2 as the anode which reported a 49.2% reduction in current density over a 12 h period of continuous electrolysis without any switching of the polarity of the cell. In the same study it was demonstrated that FeCoNi oxyhydroxide nanosheets could reversibly switch between the OER and HER, over a period of 6 h.[24] Here, we have shown that the Pt–Ni electrode can tolerate much more demanding conditions over a 24 h period with the added advantage of not using Co which has usage concerns from a geopolitical perspective.[25]

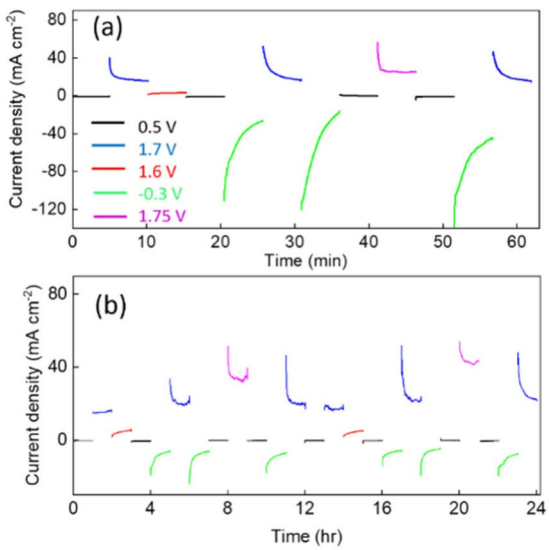

Figure 4. Stability measurements as a function of the applied potential (vs. RHE) for a) 1 hour with 5 mins step duration and b) 24 hours with 1 hour step duration.

2.2. Catalyst Characterization

To gain an insight into the Pt–Ni sample, Sample S-2 (electrodeposited Pt) was investigated rather than the Pt RDE to facilitate XPS, SEM and TEM measurements which are difficult to undertake using a RDE. This is assumed to be valid as the electrochemical activity of both samples (S-2 and S-4) were comparable and the formation of Ni on Pt has a beneficial effect for the OER and HER (Figure 2). Figure 5a shows Pt electrodeposited onto a GC electrode followed by cathodic activation in 1 M H_2SO_4. Spherical Pt particles are observed that are ca. 2 μm in diameter, with evidence of some smaller particles of ca. 0.5 μm diameter. This type of deposit is typical for Pt electrodeposited onto GC electrodes.[7b] Upon electroless deposition of Ni, the size of the particles does not change but the appearance of smaller particles on the surface of some of the larger deposits becomes evident. EDX mapping of the particles (Figure 5d) shows that Ni decorates the surface of all the Pt particles while the background GC surface does not show the presence of Ni. After electrochemical cycling (5 cycles between −0.3 and 1.6 V vs RHE) the surface decoration on the particles becomes more pronounced on many of the particles and EDX mapping shows that Pt and Ni are associated with each other across the sample.

The sample was characterized by XPS where the observed peak positions for Pt 4f were 70.9 eV and 74.2 eV for Pt $4f_{7/2}$ and Pt $4f_{5/2}$ core levels, respectively (Figure 6a), confirming the pure metallic state of electrodeposited Pt.[26] The asymmetry in the peaks and contribution at higher binding energies are due to the formation of some surface oxide. However, when the sample was activated by cathodic polarization, the Pt XPS spectrum changed significantly. Additional peaks were measured at 71.9 and 76.6 eV indicating Pt^{2+} formation, most likely in the form of PtO (Figure 6b)[27] while the contributions at 70.8 and 74.1 eV illustrate the underlying presence of Pt^0. This indicates that a cathodically polarized Pt surface is prone to significant oxidation upon exposure to the atmosphere and

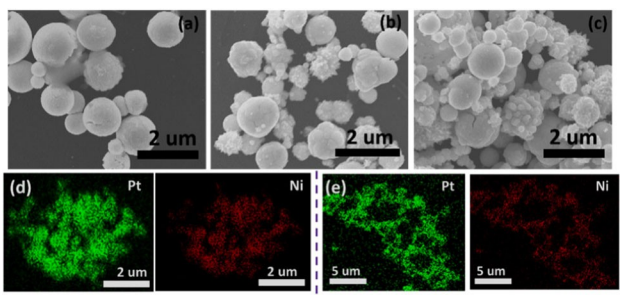

Figure 5. SEM images of a) activated Pt, b) Ni deposited on activated Pt (Sample S-2) and c) sample S-2 after electrochemical water splitting; EDS mapping showing Pt and Ni d) for sample S-2 and e) sample S2 after electrochemical water splitting.

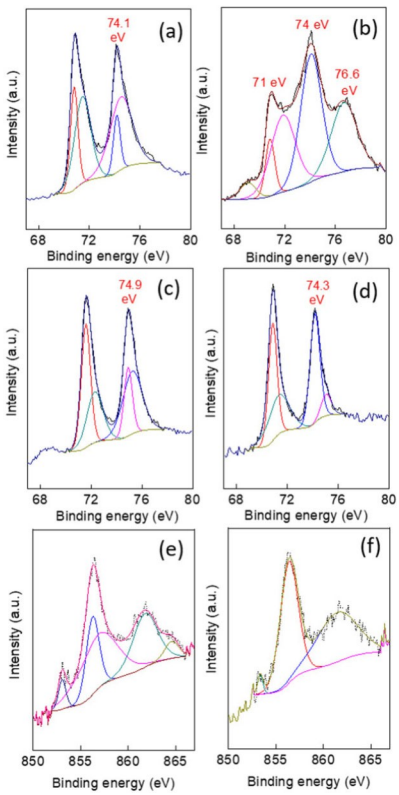

Figure 6. XPS spectra of Pt 4f for a) electrodeposited Pt, b) activated Pt, c) activated sample after electroless Ni deposition (Sample S-2), d) sample S-2 after electrochemical water splitting and Ni 2p spectra for e) sample S-2 and f) sample S-2 after electrochemical water splitting.

confirms its high reactivity. Figure 6c shows the Pt 4f spectrum for the activated electrode after reaction with the nickel salt. The significant oxidation of the surface has been prevented and the spectrum resembles that of electrodeposited Pt (Figure 6a). However, there is a 0.8 eV shift in the peak positions indicating that an electronic effect has occurred which could indicate alloy formation between Pt and Ni.[8c,26] The Ni 2p XPS spectrum for this sample (Figure 6e) shows the presence of metallic Ni by the peak at a binding energy of 852.9 eV, which is consistent with the formation of a Pt–Ni alloy,[28] while the peaks at 852.8 and 856.1 eV indicate that Ni is also in the Ni^{2+} oxidation state, consistent with the formation of $Ni(OH)_2$ and/or NiO,[29] as reported for Pt_3Ni nanowires,[8c] and Pt_3Ni octahedra.[30]

After electrochemical water splitting (cycling between the HER and OER regions) the Pt 4f spectrum does not show a significant change (Figure 6d), and a shift in the peak positions is maintained compared to unmodified Pt, indicating preservation of the electronic effect between Pt and Ni. The Ni 2p spectrum (Figure 6f) shows a slight change in that the Ni^0 peak is diminished which is expected due to formation of an oxide/hydroxide layer during the OER and the surface is dominated by the Ni^{2+} oxidation state. The XPS data indicated the composition of the electrode changed from Pt_2Ni before electrochemical water splitting to $Pt_{2.5}Ni$ after this process. The O 1s spectra are shown in Figure S4 where Pt shows evidence of some oxidation on the surface, typical of OH groups. After cathodic polarization the deconvoluted O 1s spectrum (Figure S4-b) shows peaks at 533.6, 531.6 and 529.4 eV corresponding to adsorbed H_2O, Pt-OH and Pt–O groups respectively, which is consistent with the Pt 4f spectrum indicating the reactivity of activated Pt. Upon decoration with Ni the O 1s spectrum (Figure S4-c) resembles that of the electrodeposited Pt (Figure S4-a) and the surface is dominated by a contribution from OH surface groups. After electrochemical water splitting (Figure S4-d) the presence of OH groups is maintained but there is emergence of a peak at 529.4 eV attributed to metal-oxygen bonding. In this case it is expected to be the formation of NiO as our previous work using synchrotron X-ray absorption near edge structure mapping of $Ni(OH)_2$ electrodes showed that there is some conversion of $Ni(OH)_2$ into NiO after the OER.[11c]

The HRTEM image (Figure 7a) of the Ni–Pt electrocatalyst shows a material with distinct lattice spacings of 0.22, 0.35 and 0.27 nm which correspond to a Pt_3Ni (111) alloy,[28–29] Ni metal[30] and β-$Ni(OH)_2$,[33] respectively. The SAED pattern (inset Figure 7a) also shows the presence of some Pt_3Ni(111). Interestingly, the sample after electrochemical water splitting showed large areas with a very uniform lattice spacing of 0.22 nm corresponding to the Pt_3Ni (111) alloy consistent with the SAED pattern. Scanning TEM dark field (STEM-DF) imaging in combination with EDX elemental mapping shows the homogeneous distribution of Pt and Ni across the nanomaterials both before and after electrochemical water splitting (Figure S5). The homogeneous distribution of both elements is maintained, and no segregation was observed after electrochemical water splitting reactions, indicating the compositional stability of this catalyst, even though some structural changes are observed in terms of further Pt–Ni alloy formation. The XPS results indicated that $Pt_{2.5}Ni$ is formed in this process and therefore Pt_3Ni alloy formation is not uniformly created across the surface of the Pt nanoparticles as Ni also exists in the form of $Ni(OH)_2$.

2.3. Formation Mechanism for Pt–Ni

The formation mechanism for Pt-Ni is illustrated in Figure 8. Upon cathodic polarization, highly disrupted active states or metastable states of Pt are produced as reported previously (Step A→B).[14,16,32] These sites are highly reactive and are prone to oxidation as seen from the XPS data (Figure 6b). However, if the activated surface is rapidly exposed to a nickel nitrate solution then the Pt surface reacts with the salt resulting in

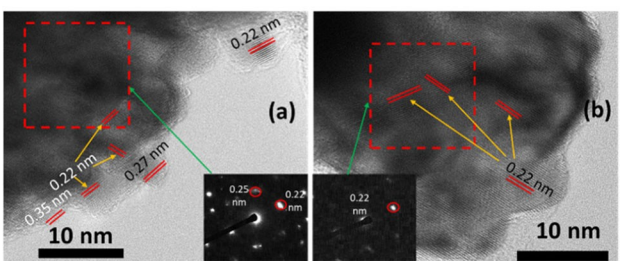

Figure 7. HR-TEM images of Ni–Pt catalyst a) as synthesized and b) after electrochemical water splitting.

oxidation of Pt where the liberated electrons are donated to the Ni^{2+} species in solution, thereby reducing it to Ni metal (Step B→C). There will also be a competing reaction with surface oxidation to Pt oxide in an aqueous environment as seen in the XPS data where surface Pt oxide is also evident (Figure 6c), in addition to the presence of Ni. Interestingly this step (B→C) results in some Pt–Ni alloy formation on the surface of the electrode as seen in the HRTEM images (Figure 7a). The distribution of Ni over the entire Pt surface is homogeneous (Figure 5d) and is consistent with a similar strategy used by us previously to fabricate a Ag decorated Au substrate.[13]

The driving force for the electroless deposition of Ni onto Pt is not attributed to adsorbed hydrogen acting as a reductant as the standard reduction potential values for the Ni^{2+}/Ni^0 (-0.27 V vs SHE) and H^+/H (0 V vs SHE) couples indicate this is thermodynamically not feasible and is therefore postulated to be due the creation of highly active sites that are readily oxidized. Upon repetitive cycling between the HER and OER regions, the extent of Pt–Ni alloy formation in the form of Pt_3Ni was seen to increase (Figure 7b) but did not occur exclusively over the entire Pt surface as regions of $Ni(OH)_2$ exist. It is known that Pt undergoes a place exchange reaction[33] upon oxidation whereby oxygen atoms exchange with surface Pt atoms to generate a layered structure with subsurface oxygen atoms existing below the Pt atoms (Step C→D→E). Upon electrochemically reducing the oxide in the reverse sweep (Step E→F) vacancies are created and a disrupted Pt surface is the result. It is envisaged that when Ni is present on the Pt surface that this place exchange reaction occurs at both the Pt and Ni atoms. Upon reduction and cleavage of the metal-oxide bonds (Step E→F) the possibility of further Pt–Ni alloy formation may occur as seen by the TEM images in Figure 7b. It is known that repetitive oxidation and reduction of Pt results in a highly disrupted surface where adatoms of Pt are created all over the surface.[14,32a,34] A similar process is postulated to occur here which results in a homogeneous distribution of Ni on Pt which results in alloying between the two metals. The overall formation mechanism is outlined in Figure 8. The resultant material comprises of partial decoration of Pt_3Ni on Pt with also Ni in the oxidized state of $Ni(OH)_2$.

This composition explains the bifunctionality of this material towards the OER and the HER. It is known that Ni oxides/hydroxides are highly active for the OER[11c,35] which is demonstrated here (Figure 2a). However, the increased activity for the Pt–Ni catalyst compared to Pt for the HER is interesting. This is not due to a change in surface area as the cyclic voltammogram recorded for Pt (Sample S-0) and Pt–Ni (Sample S-4) did not show any change in the magnitude of the H_{ads}/H_{des} region which is directly related to the surface area of the electrode (Figure 1a). Therefore, the increased HER activity must be related to the presence of Ni on the surface. This is consistent with previous reports which showed that the presence of Ni on Pt(111) improved HER performance compared to Pt(111) due to the benefit of Ni facilitating the water dissociation step.[36] It was also reported that the creation of a $Ni(OH)_2$-Pt interface is critical for this step under alkaline conditions,[39] where subsequently Pt sites at the catalyst surface are available for H_{ads} and recombination thereby facilitating the HER. This improvement in the Volmer step of the HER results in enhanced current densities at these types of electrodes.[12] This emphasizes the important role that metal/metal oxide interfaces play in facilitating high performance water splitting reactions.[40]

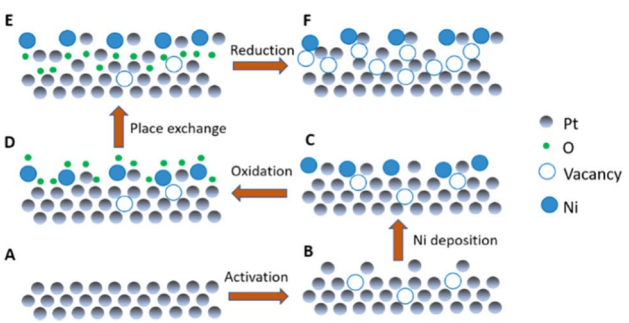

Figure 8. Illustration of the formation mechanism of a Pt–Ni electrocatalyst.

2.4. Fuel Cell Relevant Electrocatalytic Reactions

Given that some Pt_3Ni alloy material is formed on the surface of the Pt electrode, it was investigated for the ORR as that particular alloy has been extensively studied for this reaction.[8a,c,26, 39] Figure 9a shows linear sweep voltammograms for samples S-0 and S-4 (after repetitive cycling between the HER and OER regions) for the ORR where the onset potential values for Pt and Pt–Ni are comparable. However, in the mixed kinetic-diffusion controlled region between 1.0 and 0.8 V there is a more rapid increase in current recorded at the Pt–Ni catalyst compared to Pt until a diffusion limited value of ca.

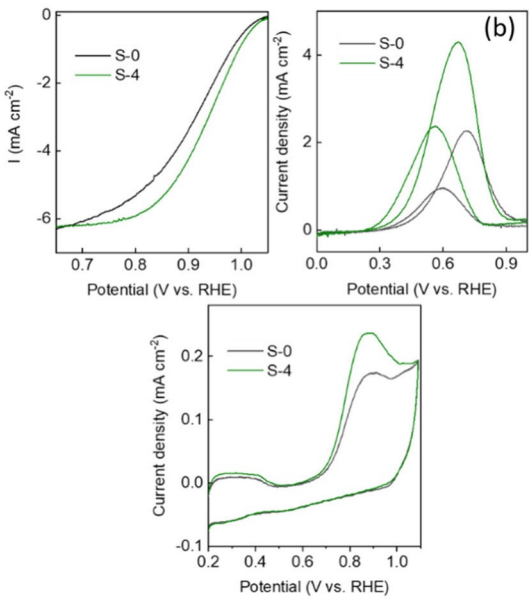

Figure 9. Cyclic voltammograms recorded at 20 mV s^{-1} in 1 M KOH for samples S-0 and S-4 (after cycling between the HER and OER regions) for a) the ORR at 1500 rpm, b) 1 M ethanol, and c) 0.5 M NH_4OH.

6.2 mA cm^{-2} is reached for both materials. This type of shift in the half wave potential to more positive values is typical for Pt_3Ni alloy materials compared to Pt. This is related to weaker binding of oxygen to the Pt–Ni catalyst compared to Pt (Figure 1a) which facilitates the ORR.

The ORR is highly important for fuel cell reactions and therefore the catalyst was also investigated for other relevant reactions such as the ethanol oxidation reaction (EOR) (Figure 9b). Pt–Ni shows an earlier onset potential of 0.27 V compared to 0.32 V for Pt indicating an enhanced electrocatalytic effect. This is also reflected in increased current density at the anodic peak for ethanol oxidation of 4.3 and 2.3 mA cm^{-2} for Pt–Ni (at 0.67 V) and Pt (at 0.72 V) respectively. On the reverse sweep ethanol is re-oxidized on the catalyst surface once the monolayer oxide is removed and shows an enhanced response at Pt–Ni compared to Pt. This reverse peak is not due to the oxidation of accumulated carbonaceous species on the surface as the forward and reverse current responses are from the same chemical origin and not indicative of poisoning effects.[42] The XPS measurements also indicated the presence of $Ni(OH)_2$ on the surface of the catalyst. which is also an effective catalyst for the EOR,[43] however the onset potential is more positive and is associated with the Ni^{2+}/Ni^{3+} redox couple at ca. 1.3 V vs RHE mediating the electrocatalytic reaction. At the Pt–Ni electrode (Figure 7b) the onset potential for the EOR is significantly less positive and is associated with the Pt component of the catalyst being modified by the presence of Ni. This is consistent with single atom Ni decorated on Pt nanowires which demonstrated good EOR performance compared to Pt nanowires with an onset potential of ca. 0.34 V vs RHE.[3b] The presence of Ni, and more specifically a $Ni(OH)_2$-Pt (111) interface, was critical as CO binding compared to Pt was weaker facilitating better EOR performance.

Finally the ammonia electro-oxidation reaction was studied due to recent interest in developing a Direct Ammonia Fuel Cell, which is an attractive carbon free energy source with a high energy density of 3000 Wh/kg.[44] Cyclic voltammograms for the oxidation of 0.5 M NH_4OH in 1 M KOH are shown in Figure 9c for Pt and Pt–Ni catalysts where the peak current for Pt–Ni (0.24 mA cm^{-2}) is larger than that recorded for Pt (0.17 mA cm^{-2}). The peak potentials are the same for both materials and this appears common for Pt modified materials where the presence of additional components does not affect the peak position but the peak current values as shown with Pt/SnO_2 electrocatalysts.[44] In that work the enhancement was in part due to lower charge transfer resistance when SnO_2 was present. Feliu has studied Pt for this reaction and found that it is structure sensitive where Pt(100) sites are more active than (111) or (110) sites.[3c] It has also been shown that Pt–Ni nanocubes are more active than Pt nanocubes[45] in terms of current density but not onset potential. This is due to Ni favouring OH adsorption which is normally a competing reaction at Pt that blocks the active sites for NH_3 adsorption. Therefore, for Pt–Ni the presence of Ni allows the reaction to proceed at the now available Pt sites as OH adsorption is occurring on the Ni component.

3. Conclusions

In this work, the possibility of creating a multifunctional electrocatalyst based on Pt–Ni has been realized. The electroless deposition of Ni is facilitated by the oxidation of active Pt sites created by a cathodic polarization process. The resultant Pt–Ni electrode was investigated for overall water splitting where bifunctional activity was observed. The OER occurs at the $Ni(OH)_2$ species on the electrode surface while the HER occurs at the Pt sites where the presence of Ni promotes the water dissociation step resulting in higher current densities compared to Pt. Promisingly, an accelerated ageing test illustrated the tolerance of this catalyst to rapid changes in potential that may occur if an alkaline electrolyser is directly integrated with an intermittent renewable energy source. Upon electrochemical cycling, the Pt–Ni electrode showed evidence for the formation of Pt_3Ni on the surface of the Pt electrode which opened up fuel cell relevant reactions such as the ORR where enhanced activity compared to Pt was observed. Ethanol and ammonia oxidation were also investigated where the presence of Ni was again found to be highly beneficial for both reactions. This simple fabrication approach may be applicable to other bimetallic compositions that would allow access to many other important reactions.

Experimental Section

Materials and Chemicals

Nickel (II) nitrate hexahydrate (Sigma Aldrich), potassium tetra chloroplatinate (K_2PtCl_4, 99.9%), absolute ethanol ($\geq$99.8%), sulfuric acid (conc.), ammonia solution, 28% (Ajax Finechem) and potassium hydroxide (ACS reagent) (Sigma-Aldrich) were used as received from the suppliers and made up with deionized water (resistivity of 18.2 MΩ cm) purified by use of a Milli-Q reagent deionizer (Millipore).

Electrochemical experiments

Electrochemical measurements were undertaken at (20 $\pm$2) °C with a BioLogic VSP workstation equipped with a Rotating Ring Disk Electrode-3 A (RRDE) in a standard three-electrode cell configuration, consisting of a working electrode, a reference electrode, and a counter electrode. The reference electrode was a leakless Ag/AgCl (eDAQ) and a carbon rod 6 mm in diameter (Thermo Fisher) was used as the counter electrode in all experiments to avoid any possible dissolution effects during long term electrocatalytic reactions.36 For voltammetric experiments, a platinum rotating disk electrode (RDE) (3 mm diameter) or glassy carbon RDE (3 mm diameter) from BAS Inc (Japan) were used as the working electrode. Prior to each experiment, the surface of each electrode was mechanically polished with 0.5 μm-sized alumina powder on a Microcloth pad, rinsed in Milli-Q water, sonicated in diluted nitric acid for 2 mins and then again sonicated in ethanol for 2 mins. These procedures were repeated several times and finally the electrode surface was rinsed thoroughly with Milli-Q water to ensure no impurities were left on the surface. For all electrochemical experiments, except the ORR, the electrolyte solution was purged for 10 mins with nitrogen prior to performing any experiments to remove dissolved oxygen from the solution. For ORR

experiments the electrolyte was purged for 20 mins with high purity O_2 (Supagas, ultrahigh purity). For HER and OER experiments *iR* correction was applied to all cyclic voltammograms that were recorded using a rotation rate of 500 rpm. For all electrochemical data the potential has been converted to the RHE scale via $E_{RHE} = E_{Ag/AgCl} + 0.059 \times pH + E^0_{Ag/AgCl}$ [V]. The current density reported in this work was normalized to the geometric surface area of the electrodes.

Pt working electrode preparation

Table 1 shows the different Pt electrodes that were prepared to compare their electrochemical performance. Sample S-0 is the Pt RDE electrode that is cleaned by the above procedure. Sample S-1 is the Pt RDE electrode that is cleaned by the above procedure followed by activation of the Pt electrode in acidic media (1 M H_2SO_4) at a constant potential of −0.75 V (vs Ag/AgCl) rotated at 500 rpm and for an activation time that was optimized based on OER and HER performance. Figure S1 shows the current response recorded during Pt activation in 1 M sulfuric acid for 1 min using this chronoamperometric technique. Sample S-4 is a Pt RDE that is activated followed by immediate immersion in de-gassed double deionized water followed by instant immersion in 2–10 mM nickel nitrate solution. Electrode contact with air was minimized to prevent air oxidation of the electrode and the electrode was gently rinsed with milli-Q water to wash the nickel nitrate solution residue from the electrode surface. The electrode was then ready for electrochemical characterization. Sample S-3 was also prepared in the same way but without the Pt activation step. Sample S-2 is Pt electrodeposited onto a GC electrode that is then cathodically activated and immersed in nickel nitrate solution in the same way as sample S-4 and is used to perform surface characterization studies given the difficulty in inserting RDE electrodes into SEM and XPS instruments. To prepare the Pt electrodeposited GC electrode, the GC RDE was first cleaned using the method described above. Platinum was electrodeposited from a solution of 5 mM K_2PtCl_4 using chronoamperometry at a constant potential of −1.2 V (vs Ag/AgCl) for one minute. The electrodeposited Pt was activated using the same procedure described above for the Pt RDE followed by immersion in the nickel nitrate solution using the same procedure for sample S-4.

Material characterisation

X-ray photoelectron spectroscopy measurements were carried out using an AXIS Supra instrument (Kratos Analytical, UK) incorporating a monochromatic Al Kα X-ray source with a 15 mA emission current and total power of 225 W, which provided 300 μm ×700 μm area of interest. All the measurements were done using the charge neutralizer as a default. Wide scans were recorded at an analyser pass energy of 160 eV with 0.5 eV steps and 300 ms dwell time. Narrow high-resolution scans for Ni 2p, Pt 4f, O 1s and C 1s were taken at 20 eV pass energy, 0.2 eV steps, and 300 ms dwell time. The base pressure in the analysis chamber was 1.0×10^{-8} torr. One sweep was conducted for a wide scan whereas at least two sweeps were taken for narrow scans. Data analysis was done in CasaXPS licenced software following Shirley baseline with Kratos library Relative Sensitivity Factors (RSFs). SEM and EDX were performed on a JEOL 7001F instrument at an operating voltage of 5 kV and 15 kV, respectively. HRTEM, SAED, STEM-DF, and STEM-EDX measurements were performed using a JEOL 2100 TEM instrument operating at an accelerating voltage of 200 kV. The JEOL 2100 machine was equipped with a high-sensitivity OXFORD 80 mm^2 silicon drift X-ray detector for accurate elemental analysis and JEOL BF/DF detectors for STEM imaging.

Acknowledgements

A.O.M. acknowledges funding from the Australian Research Council (DP180102869). The authors acknowledge the instrumentation and technical support of the QUT Central Analytical Research Facility operated by the Institute for Future Environments. A.O.M., J.L. acknowledge the Australian Renewable Energy Agency for funding as part of the Research and Development Program-Renewable Hydrogen for Export.

Conflict of Interest

The authors declare no conflict of interest.

Keywords: water splitting · electrocatalysis · Pt–Ni alloy · ORR · ammonia oxidation

[1] a) D. Hara, *ECS Trans.* **2019**, *91*, 3–7; b) G. Glenk, S. Reichelstein, *Nat. Energy* **2019**, *4*, 216–222; c) R.-H. Lin, Y.-Y. Zhao, B.-D. Wu, *Int. J. Hydrogen Energy* **2020**, *45*, 20164–20175.
[2] I. Staffell, D. Scamman, A. Velazquez Abad, P. Balcombe, P. E. Dodds, P. Ekins, N. Shah, K. R. Ward, *Energy Environ. Sci.* **2019**, *12*, 463–491.
[3] a) H. Yin, S. Zhao, K. Zhao, A. Muqsit, H. Tang, L. Chang, H. Zhao, Y. Gao, Z. J. N. C. Tang, *Nat. Commun.* **2015**, *6*, 1–8; b) M. Li, K. Duanmu, C. Wan, T. Cheng, L. Zhang, S. Dai, W. Chen, Z. Zhao, P. Li, H. Fei, Y. Zhu, R. Yu, J. Luo, K. Zang, Z. Lin, M. Ding, J. Huang, H. Sun, J. Guo, X. Pan, W. A. Goddard, P. Sautet, Y. Huang, X. Duan, *Nat. Can.* **2019**, *2*, 495–503; c) F. Vidal-Iglesias, N. Garcıa-Aráez, V. Montiel, J. Feliu, A. Aldaz, *Electrochem. Commun.* **2003**, *5*, 22–26; d) A. Mahata, A. S. Nair, B. Pathak, *Catal. Sci. Technol.* **2019**, *9*, 4835–4863; e) N. S. Marinkovic, M. Li, R. R. Adzic, *Topics in Curr. Chem.* **2019**, *377*, 11; f) W. Li, D. Wang, Y. Zhang, L. Tao, T. Wang, Y. Zou, Y. Wang, R. Chen, S. Wang, *Adv. Mater.* **2020**, *32*, 1907879; g) K. Siddharth, Y. Hong, X. Qin, H. J. Lee, Y. T. Chan, S. Zhu, G. Chen, S.-I. Choi, M. Shao, *Appl. Cat. B* **2020**, *269*, 118821.
[4] M. D. Zott, P. Garrido-Barros, J. C. Peters, *ACS Catal.* **2019**, *9*, 10101–10108.
[5] B. H. R. Suryanto, H.-L. Du, D. Wang, J. Chen, A. N. Simonov, D. R. MacFarlane, *Nat. Can.* **2019**, *2*, 290–296.
[6] a) X. Ren, Q. Lv, L. Liu, B. Liu, Y. Wang, A. Liu, G. Wu, *Sustainable Energy Fuels* **2020**, *4*, 15–30; b) K. Sasaki, K. A. Kuttiyiel, R. R. Adzic, *Curr. Opinion Electrochem.* **2020**, *21*, 368–375.
[7] a) S. Themsirimongkon, T. Sarakonsri, S. Lapanantnoppakhun, J. Jakmunee, S. Saipanya, *Int. J. Hydrogen Energy* **2019**, *44*, 30719–30731; b) B. Plowman, M. Abdelhamid, S. Ippolito, V. Bansal, S. Bhargava, A. O'Mullane, *J. Solid State Electrochem.* **2014**, *18*, 3345–3357; c) J. Zhang, H. Li, J. Ye, Z. Cao, J. Chen, Q. Kuang, J. Zheng, Z. Xie, *Nano Energy* **2019**, *61*, 397–403.
[8] a) Z. Yang, J. Wang, X. Yu, *Chem. Phys. Lett.* **2010**, *499*, 83–88; b) V. R. Stamenkovic, B. Fowler, B. S. Mun, G. Wang, P. N. Ross, C. A. Lucas, N. M. Marković, *Science* **2007**, *315*, 493; c) M. Gong, Z. Deng, D. Xiao, L. Han, T. Zhao, Y. Lu, T. Shen, X. Liu, R. Lin, T. Huang, G. Zhou, H. Xin, D. Wang, *ACS Catal.* **2019**, *9*, 4488–4494.
[9] a) I. Ledezma-Yanez, W. D. Z. Wallace, P. Sebastián-Pascual, V. Climent, J. M. Feliu, M. T. M. Koper, *Nat. Energy* **2017**, *2*, 17031; b) G. Wang, J. Parrondo, C. He, Y. Li, V. Ramani, *J. Electrochem. Soc.* **2017**, *164*, F1307-F1315.
[10] R. Subbaraman, D. Tripkovic, D. Strmcnik, K.-C. Chang, M. Uchimura, A. P. Paulikas, V. Stamenkovic, N. M. Markovic, *Science* **2011**, *334*, 1256–1260.
[11] a) I. Roger, M. A. Shipman, M. D. Symes, *Nat. Chem. Rev.* **2017**, *1*, 0003; b) K. Zhang, X. Xia, S. Deng, Y. Zhong, D. Xie, G. Pan, J. Wu, Q. Liu, X. Wang, J. Tu, *Nano-Micro Lett.* **2019**, *11*, 21; c) R. Agoston, M. Abu Sayeed, M. W. M. Jones, M. D. de Jonge, A. P. O'Mullane, *Analyst* **2019**, *144*, 7318–7325.
[12] R. Subbaraman, D. Tripkovic, K.-C. Chang, D. Strmcnik, A. P. Paulikas, P. Hirunsit, M. Chan, J. Greeley, V. Stamenkovic, N. M. Markovic, *Nat. Mater.* **2012**, *11*, 550–557.

[13] B. J. Plowman, M. R. Field, S. K. Bhargava, A. P. O'Mullane, *ChemElectroChem* **2013**, *1*, 76–82.
[14] G. Liu, D.-Q. Feng, W. Zheng, T. Chen, D. Li, *Chem. Commun.* **2013**, *49*, 7941–7943.
[15] a) L. D. Burke, M. A. Horgan, L. M. Hurley, L. C. Nagle, A. P. O'Mullane, *J. Appl. Electrochem.* **2001**, *31*, 729–738; b) V. Díaz, S. Real, E. Téliz, C. F. Zinola, M. E. Martins, *Int. J. Hydrogen Energy* **2009**, *34*, 3519–3530; c) A. P. O'Mullane, S. K. Bhargava, *Electrochem. Commun.* **2011**, *13*, 852–855.
[16] A. I. Yanson, P. Rodriguez, N. Garcia-Araez, R. V. Mom, F. D. Tichelaar, M. T. M. Koper, *Angew. Chem. Int. Ed.* **2011**, *50*, 6346–6350; *Angew. Chem.* **2011**, *123*, 6470–6474.
[17] a) P. Daubinger, J. Kieninger, T. Unmüssig, G. A. Urban, *Phys. Chem. Chem. Phys.* **2014**, *16*, 8392–8399; b) V. Diaz, C. F. Zinola, *J. Coll. Inter. Sc.* **2007**, *313*, 232–247.
[18] N. Danilovic, R. Subbaraman, D. Strmcnik, K.-C. Chang, A. P. Paulikas, V. R. Stamenkovic, N. M. Markovic, *Angew. Chem. Int. Ed.* **2012**, *51*, 12495–12498; *Angew. Chem.* **2012**, *124*, 12663–12666.
[19] R. D. L. Smith, C. P. Berlinguette, *J. Am. Chem. Soc.* **2016**, *138*, 1561–1567.
[20] F. J. Pérez-Alonso, C. Adán, S. Rojas, M. A. Peña, J. L. G. Fierro, *Int. J. Hydrogen Energy* **2015**, *40*, 51–61.
[21] D. F. van der Vliet, C. Wang, D. Tripkovic, D. Strmcnik, X. F. Zhang, M. K. Debe, R. T. Atanasoski, N. M. Markovic, V. R. Stamenkovic, *Nat. Mater.* **2012**, *11*, 1051–1058.
[22] M. Görlin, P. Chernev, J. Ferreira de Araújo, T. Reier, S. Dresp, B. Paul, R. Krähnert, H. Dau, P. Strasser, *J. Am. Chem. Soc.* **2016**, *138*, 5603–5614.
[23] Y. Uchino, T. Kobayashi, S. Hasegawa, I. Nagashima, Y. Sunada, A. Manabe, Y. Nishiki, S. Mitsushima, *Electrocatal.* **2018**, *9*, 67–74.
[24] Q. Zhang, N. M. Bedford, J. Pan, X. Lu, R. Amal, *Adv. Energy Mater.* **2019**, *9*, 1901312.
[25] E. A. Olivetti, G. Ceder, G. G. Gaustad, X. Fu, *Joule* **2017**, *1*, 229–243.
[26] M. Peuckert, F. P. Coenen, H. P. Bonzel, *Electrochim. Acta* **1984**, *29*, 1305–1314.
[27] K. N. Han, C. A. Li, M.-P. N. Bui, X.-H. Pham, B. S. Kim, Y. H. Choa, G. H. Seong, *Sens. Act. B* **2012**, *174*, 406–413.
[28] H. C. Lee, B. M. Kim, C. K. Jeong, R. Toyoshima, H. Kondoh, T. Shimada, K. Mase, B. Mao, Z. Liu, H. Lee, C.-Q. Huang, W. X. Li, P. N. Ross, B. S. Mun, *Catal. Today* **2016**, *260*, 3–7.
[29] J. Wang, S. Mao, Z. Liu, Z. Wei, H. Wang, Y. Chen, Y. Wang, *ACS Appl. Mater. Interfaces* **2017**, *9*, 7139–7147.
[30] X. Huang, Z. Zhao, L. Cao, Y. Chen, E. Zhu, Z. Lin, M. Li, A. Yan, A. Zettl, Y. M. Wang, X. Duan, T. Mueller, Y. Huang, *Science* **2015**, *348*, 1230.
[31] C. Zhang, S. N. Oliaee, S. Y. Hwang, X. Kong, Z. Peng, *Nano Lett.* **2016**, *16*, 164–169.
[32] a) K. Jayasayee, J. A. R. V. Veen, T. G. Manivasagam, S. Celebi, E. J. M. Hensen, F. A. de Bruijn, *Appl. Catal. B* **2012**, *111–112*, 515–526; b) H. Zhang, B. Yi, S. Jiang, Y. Zeng, Z. Shao, *ChemElectroChem* **2017**, *4*, 1436–1442.
[33] M. A. Sayeed, J. F. S. Fernando, A. P. O'Mullane, *Adv. Sustainable Syst.* **2018**, *2*, 1800019.
[34] a) L. D. Burke, L. M. Kinsella, A. M. O'Connell, *Russ. J. Electrochem.* **2004**, *40*, 1105–1114; b) L. D. Burke, L. M. Hurley, *J. Solid State Electrochem.* **2000**, *4*, 353–362; c) L. D. Burke, L. M. Hurley, A. P. O'Mullane, *Proc. Electrochem. Soc.* **1999**, *98–26*, 215–224; d) L. D. Burke, L. M. Hurley, *Electrochim. Acta* **1999**, *44*, 3451–3473.
[35] a) A. A. Topalov, S. Cherevko, A. R. Zeradjanin, J. C. Meier, I. Katsounaros, K. J. J. Mayrhofer, *Chem. Sci.* **2014**, *5*, 631–638; b) H. A. Baroody, G. Jerkiewicz, M. H. Eikerling, *J. Chem. Phys.* **2017**, *146*, 144102; c) H. Angerstein-Kozlowska, B. E. Conway, B. Barnett, J. Mozota, *J. Electroanal. Chem. Interfacial Electrochem.* **1979**, *100*, 417–446.
[36] L. D. Burke, J. A. Collins, M. A. Horgan, L. M. Hurley, A. P. O'Mullane, *Electrochim. Acta* **2000**, *45*, 4127–4134.
[37] a) P. Kanagavalli, R. Sudha, S. Boopathi, S. S. Kumar, *Electrochem. Commun.* **2017**, *82*, 61–65; b) M. E. Lyons, M. P. Brandon, *J. Electroanal. Chem.* **2010**, *641*, 119–130.
[38] S. Xue, R. W. Haid, R. M. Kluge, X. Ding, B. Garlyyev, J. Fichtner, S. Watzele, S. Hou, A. S. Bandarenka, *Angew. Chem. Int. Ed.* **2020**, *59*, 10934–10938.
[39] Z. Zhao, H. Liu, W. Gao, W. Xue, Z. Liu, J. Huang, X. Pan, Y. Huang, *J. Am. Chem. Soc.* **2018**, *140*, 9046–9050.
[40] A. P. O'Mullane, *J. Phys. Energy* **2020**, *2*, 041001.
[41] Y. Tan, J. Fan, G. Chen, N. Zheng, Q. Xie, *Chem. Commun.* **2011**, *47*, 11624–11626.
[42] A. M. Hofstead-Duffy, D.-J. Chen, S.-G. Sun, Y. J. Tong, *J. Mater. Chem.* **2012**, *22*, 5205–5208.
[43] P. E. Sharel, D. Liu, R. A. Lazenby, J. Sloan, M. Vidotti, P. R. Unwin, J. V. Macpherson, *J. Phys. Chem. C* **2016**, *120*, 16059–16068.
[44] J. R. Barbosa, M. N. Leon, C. M. Fernandes, R. M. Antoniassi, O. C. Alves, E. A. Ponzio, J. C. M. J. A. C. B. E. Silva, *Appl. Catal. B* **2020**, *264*, 118458.
[45] Y. T. Chan, K. Siddharth, M. Shao, *Nano Res.* **2020**, *13*, 1920–1927.

Manuscript received: October 1, 2020
Revised manuscript received: October 12, 2020
Accepted manuscript online: October 12, 2020